

A LONG TERM 2D VERTICAL MODELLING STUDY OF CO₂ STORAGE AT SLEIPNER (NORTH SEA) USING TOUGHREACT

Pascal Audigane⁽¹⁾, Irina Gaus⁽¹⁾, Karsten Pruess⁽²⁾, Tianfu Xu⁽²⁾

⁽¹⁾ BRGM, French Geological Survey, 3 Av. Claude Guillemin, BP 6009
45060 ORLEANS Cedex 2 (FRANCE)

⁽²⁾ LBNL, Lawrence Berkeley National Laboratory, Earth Sciences Division, University of California, One
cyclotron Road, MS 90-1116 Berkeley, CA 94720, USA
e-mail: p.audigane@brgm.fr

ABSTRACT

This paper presents a numerical modelling study of the long term storage of CO₂ in a saline aquifer at Sleipner in the North Sea. The simulation aims at predicting how CO₂ will be transformed because of geochemical reactions with minerals present in the host rock and with species present in the brine.

TOUGHREACT allows to simulate hydrodynamics, thermodynamics and geochemical processes involved in CO₂ storage in saline aquifers. A 2D vertical radial geometry model was used with a layered system containing a porous sand formation with four semi-permeable layers. A different mineralogy is applied for the “sand” system and for the “shale” system. Long term simulations have been performed over a time period of 10 000 years. A balance evolution of the amount of CO₂ stored (i) as supercritical phase, (ii) as dissolved in the brines and (iii) as a mineral phase due to carbonate precipitation is presented to conclude the study.

THE SLEIPNER SITE

The Sleipner West natural gas field is located in the centre of the North Sea (Norwegian block 15/9). The Utsira formation is a large sandy aquifer extending over 26100 km² located at a depth from 700 to 1000 m. Four seismic surveys have been conducted since the start of injection in 1996 at a rate of one million tons per year. Visualizations of evolution of the gas bubble have been produced before and after injection in 1999, 2001 and 2002 (Torp and Gale, 2002). The upward migration of the supercritical CO₂ due to buoyancy effects amounts to about 250 m after three years, with a lateral extension of about 600 m, and seems to have been stopped by the cap rock situated at the top of the formation (Arts and others, 2004). The seismic profiles have revealed the presence of CO₂ accumulations in a layered structure, attributed to the presence of low-permeable layers that determine the vertical and lateral extent of the CO₂ plume in the aquifer. In this modeling work, the presence of low-permeable layers was necessary to fit the seismic profiles. Therefore, we will model the Utsira formation as an assemblage of two lithologies, one called “sand” for the highly permeable part of the

porous media and one called “shale” for the low-permeable layers.

NUMERICAL METHOD

All simulations have been performed using the non-isothermal program TOUGHREACT (Xu and Pruess, 2001; Xu and others, 2006). This code was developed by introducing reactive geochemical transport into the existing multi-phase fluid and heat flow code TOUGH2 V2 (Pruess and others, 1991). The numerical method for fluid flow simulations is based on the integral finite difference method for space-discretization (Narasimhan and Witherspoon, 1976). An implicit time-weighting scheme is used for the flow and transport equations. A sequential iterative approach is used for the coupling between transport and geochemical reactions (Yeh and Tripathi, 1991).

Geometrical configuration

The Utsira formation geometry is approximated by a vertical 2D mesh with a cylindrical geometrical configuration, centered around an injection point located 155 m beneath the top of the 184 m thick formation (Figure 1a).

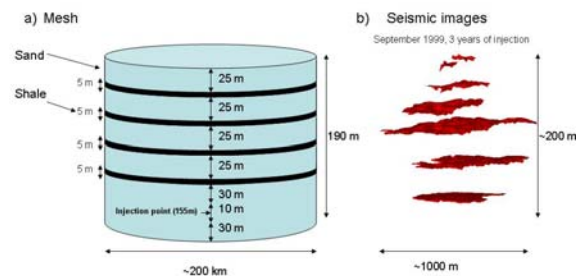


Figure 1. a) Representation of the Utsira formation by a 2D multi-layered mesh with cylindrical symmetry. b) Vertical section of the seismic images three years after CO₂ injection (SACS, 2002; Arts (2004)).

The porous media form a layered structure, composed from top to bottom of four sand layers of 25 m thickness that are separated by shale layers of 5 m thickness and a bottom sand layer of 70 m thickness into which the CO₂ is injected. The mesh

contains 22 layers in the vertical and 52 cells in the radial direction. The first cell has a radius of 10 m, and is followed by four sets of 20, 15, 10 and 5 cells with radial increments increasing in logarithmic progression out to 1, 3, 10 and 100 km from the injection point, respectively. Beyond 100 km, a last cell with an infinite volume is added with the corresponding hydrostatic pressure so that the model system would be infinite acting.

Initial and Boundary conditions

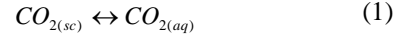
The hydrologic parameters used in the simulations are presented in Table 1. Sand and shale formations are homogeneous. Relative permeability models are fitted from core measurements (SACS2, 2002). Injection of carbon dioxide is simulated at 30 kg/sec for 25 years. The initial pressure is 90 bars at the top of the formation, which corresponds to a depth of about 900 m. Hydrostatic pressure is imposed in the outermost column of the mesh. A low salinity value of 32 g/l is assumed for the formation water both in the sand and the shale.

Table 1. Hydrogeological parameters for the 2D model of CO₂ injection at Sleipner with TOUGHREACT

	Sand	Shale
Permeability	3.0 10 ⁻¹² m ²	10 ⁻¹⁴ m ²
Porosity	0.42	0.1025
Temperature	37°C	37°C
Pore compressibility	4.510 ⁻¹⁰ Pa ⁻¹	4.5 10 ⁻¹⁰ Pa ⁻¹
Relative permeability model:		
. Liquid (Van Genuchten)		
$k_{rl} = \sqrt{S^*} \left\{ 1 - \left(1 - [S^*]^{1/m} \right)^2 \right\}^2$	$S^* = \frac{S_l - S_{lr}}{1 - S_{lr}}$	
Residual liquid saturation	$S_{lr} = 0.05$	$S_{lr} = 0.05$
Exponent	$m = 0.75$	$m = 0.75$
. Gas (Corey)		
$k_{rg} = (1 - \xi)^2 (1 - \xi^2)$	$\xi = \frac{S_l - S_{gr}}{1 - S_{lr} - S_{gr}}$	
Residual gas saturation	$S_{gr} = 0.20$	$S_{gr} = 0.20$
Capillary pressure (Van Genuchten)		
$P_{cap} = -P_0 \left([S^*]^{1/m} - 1 \right)$	$S^* = \frac{S_l - S_g}{1 - S_g}$	
Residual liquid saturation	$S_{lr} = 0.05$	$S_{lr} = 0.05$
Exponent	$m = 0.65$	$m = 0.65$
Coefficient	$P_0 = 1.43kPa$	$P_0 = 1.43kPa$

Dissolution of CO₂

During dissolution of CO₂ in the brine, gaseous and aqueous CO₂ are assumed to be in equilibrium, hence:



where subscripts “sc” and “aq” denote supercritical and aqueous CO₂, respectively. In the TOUGHREACT code, solubility of CO₂ in brine is represented by an extended version of Henry’s law allowing for salinity effects (“salting out”) as well as for fugacity corrections to CO₂ partial pressure (Pruess and García, 2002):

$$K\Gamma P = \gamma C \quad (2)$$

where K is the equilibrium constant depending on the temperature T , P is the partial pressure (bar), γ is the aqueous CO₂ activity coefficient, C is the aqueous concentration (mol/kg H₂O) and Γ is a fugacity parameter depending on pressure and temperature according to Spycher and Reed (1988).

MINERAL COMPOSITION OF THE UTSIRA FORMATION

The mineralogical composition of the Utsira Formation between 1085 and 1086 m depth has been used as a reference (Table 2). It consists mainly of quartz, k-feldspar, plagioclase, mica and calcite. Minor constituents are chlorite, zeolite, Ti-oxides, ilmenite and pyrite. Chlorite (an iron-rich variant) is used as representative of the chlorite group. Plagioclase is modeled as pure albite. The phase described as mica is considered as muscovite. Chalcedony is selected instead of quartz. The trace minerals apatite, ilmenite, pyrite, and Ti-oxides are not included in the model. Chalcedony, kaolinite as well as carbonate minerals such as calcite, siderite and disordered dolomite are commonly observed to precipitate under diagenetic circumstances and therefore are included as secondary minerals (Bjørlykke and others, 1992). Since dawsonite is also supersaturated when combining high CO₂ concentrations with the cap rock mineralogy it was decided to include it in the secondary mineral assemblage.

As there are no data for the “shale” part of the Utsira formation we will assume in this study that shale mineralogy is equivalent to the cap rock mineralogy as described by Gaus and others (2005). This mineralogical composition was based on the study of drill cuttings taken at the base of the cap rock revealing presence of quartz, undifferentiated mica, kaolinite, k-feldspar, calcite, smectite, albite, chlorite, siderite and pyrite (Bøe and Zweigel, 2001, Kemp and others, 2002). In the present study, mica is represented by muscovite and quartz by chalcedony.

Table 2. Mineralogical composition of the Utsira Sand derived from Pearce and others (1999) and its conceptualization in the geochemical model

Nordland shale composition (after Pearce and others, 1999)	Volume fraction	Minerals introduced in the model	Volume fraction
Plagioclase	0.0301	Albite-low	0.030
Calcite	0.0674	Calcite	0.067
Quartz	0.7633	Chalcedony	0.769
Chlorite	0.0133	Chlorite	0.013
Mica/Illite	0.0522	Muscovite	0.052
K-feldspar	0.0693	K-feldspar	0.069
Pyrite	0.0005	Not used	--
Ilmenite	0.0012	Not used	--
Apatite	0.0002	Not used	--
Zeolite	0.0022	Not used	--
Ti Oxides	0.0003	Not used	--
Nordland shale composition (after Pearce and others, 1999)	Volume fraction	Minerals introduced in the model	Volume fraction
Siderite	--	Siderite	0.000
Kaolinite	--	Kaolinite	0.000
Dolomite-dis	--	Dolomite-dis	0.000
Magnesite	--	Magnesite	0.000
Dawsonite	--	Dawsonite	0.000

Table 3. Mineralogical composition of the Nordland Shale derived from Bøe and Zweigel (2001) and the amounts introduced in the model

Nordland shale composition (after Bøe and Zweigel, 2001)	Volume percent	Minerals introduced in the model	Volume percent
Plagioclase	0.132	Albite-low	0.132
Calcite	0.010	Calcite	0.010
Quartz	0.228	Chalcedony	0.334
Chlorite	0.044	Chlorite	0.044
Mica/Illite	0.251	Muscovite	0.251
Kaolinite	0.195	Kaolinite	0.195
K-feldspar	0.023	K-feldspar	0.023
Siderite	0.011	Siderite	0.011
Smectite	0.09	Not used	--
Pyrite	0.016	Not used	--
Dolomite-dis	--	Dolomite-dis	0.000
Magnesite	--	Magnesite	0.000
Dawsonite	--	Dawsonite	0.000

Formation water

The composition selected for our model is similar to the Synthetic Utsira Porewater (SUP) that was used for laboratory experiments performed with Utsira sands (Czernichowski-Lauriol and others, 1996,

2002; Rochelle and Moore, 2002). This composition is taken as a starting point and is subsequently equilibrated, by means of geochemical modeling, with muscovite, albite, chalcedony, k-feldspar and chlorite, resulting in aqueous concentrations as given in Table 4.

Table 4. Initial composition of the formation water in the cap rock

Parameter	Value	Elements	Concentration (M)
Temperature (°C)	37	Al	0.4542 10 ⁻¹⁵
pH	7.67	C	0.1973 10 ⁻⁰¹
		Ca	0.3701 10 ⁻⁰³
		Cl	0.5375 10 ⁺⁰⁰
		Fe	0.4096 10 ⁻¹⁴
		K	0.1553 10 ⁻⁰²
		Mg	0.2576 10 ⁻⁰⁵
		Na	0.5439 10 ⁺⁰⁰
		S	0.1024 10 ⁻¹⁴
		Si	0.1811 10 ⁻⁰³

Kinetics of mineral precipitation and dissolution

A general kinetic rate law for mineral dissolution and precipitation is used (Lasaga, 1984):

$$r_m = k(T)_m A_m \left[1 - \left(\frac{Q_m}{K_m} \right) \right] \quad (3)$$

where m is the mineral index, r_m is the dissolution/precipitation rate (positive values indicates dissolution), A_m is the specific reactive surface area per kg of water, $k(T)_m$ is the temperature-dependent rate constant, K_m is the equilibrium constant for the mineral water reaction written for the destruction of one mole of mineral, and Q_m is the corresponding ion activity product. For all minerals the same rate law is used for precipitation and dissolution. The temperature dependence of the reaction rate constant is expressed via an Arrhenius equation:

$$k = k_{25} \left[\frac{-E_a}{R} \left(\frac{1}{T} - \frac{1}{298.15} \right) \right] \quad (4)$$

where E_a is the activation energy, k_{25} is the rate constant at 25 °C, R is the gas constant, and T is absolute temperature.

Table 5 provides the parameters and the references for the kinetics of dissolution and precipitation of all minerals used in the simulations. Specific reactive surface area remains difficult to characterize. The values used in this study correspond to those used by Xu and others (2005) and were originally taken from Sonnenthal and Spycher (2001). These values are calculated assuming a rock framework composed of a cubic array of truncated spheres. Surface areas were increased for clay minerals kaolinite and illite to account for edges in these sheet silicate minerals.

Table 5. List of kinetic rate parameters for minerals considered in the simulations

Mineral	k_{25} (mol m ⁻² s ⁻¹)	Ea (KJ/mol)	Surface area (cm ² /g)
Calcite	Equilibrium	--	--
Magnesite	Equilibrium	--	--
Dawsonite	Equilibrium	--	--
Siderite	1.26 10 ⁻⁹	62.76	9.8
Albite	1.00 10 ⁻¹²	67.83	9.8
Chalcedony	1.26 10 ⁻¹⁴	87.50	9.8
Chlorite	2.51 10 ⁻¹²	62.76	9.8
Kaolinite	1.00 10 ⁻¹³	62.76	151.6
Illite	1.00 10 ⁻¹³	62.76	151.6
K-feldspar	1.00 10 ⁻¹²	57.78	9.8
Dolomite-dis	1.26 10 ⁻⁹	62.76	9.8

SIMULATION RESULTS

Short term simulation results (injection period, 25 years)

Gas saturations and mass fractions of dissolved CO₂ (mass of CO₂ dissolved divided by mass of aqueous phase) are plotted in Figure 2 and at the end of the injection period (25 years). The gas bubble representing the supercritical CO₂ extends laterally about 300 m away from the injection point, consistent with the seismic observations. The presence of the four intra-shale aquifers gives rise to CO₂ accumulations at four different depths and slows the upward migration of CO₂. The dissolution of gas in the brine produces a maximum dissolved CO₂ mass fraction of 0.052. CO₂ dissolution slightly increases brine density and gives rise to a negative (downward) buoyancy force. At the end of the 25 year injection period, a slight downward migration of the brine enriched in CO₂ can be noted, especially near the top and between 120 m depth and the bottom of the formation.

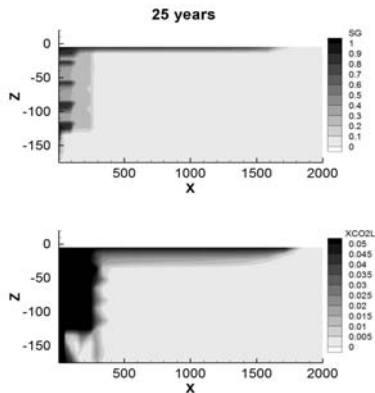


Figure 2. Gas saturations (SG) and mass fractions of dissolved CO₂ in the liquid phase (XCO₂L), after 25 years of injection.

Dissolution of CO₂ makes the brine more acidic. pH drops to a value of 5.13 inside the gas bubble, which results from buffering due to calcite dissolution (Figure 3).

The dissolution of calcite is less pronounced in the shales (~5 moles per m³ of rock) than in the sands (up to 20 moles). Calcite precipitates below each shale layer at the interface between the CO₂ saturated brine and the initial brine, due to mixing of different waters in these regions.

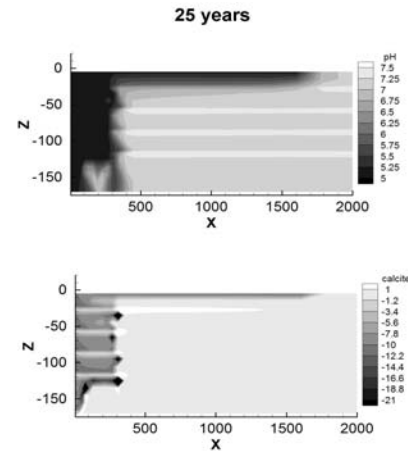


Figure 3. pH and calcite dissolution (in mol/kg³ of medium) at the end of 25 year CO₂ injection period. The negative sign corresponds to mineral dissolution.

Minor alumino-silicate alteration such as chlorite, albite and muscovite dissolution is also observed during the injection period (results not shown). Also, a small amount of reactions occurs in regions not affected by CO₂ injection. This corresponds to a slight deviation of initial speciation from equilibrium. Changes in porosity remain minor (less than 1%), indicating a weak overall chemical reactivity in the media.

Long term simulation results

Hydrodynamics

Long-term simulations of gas bubble evolution and dissolved carbon dioxide are shown in Figure 4. After injection, the upward migration of the supercritical CO₂ occurs quickly, and most of the supercritical CO₂ accumulates just below the cap rock, except for the residual CO₂ that is trapped in sediments. The CO₂ plume extends to a maximum radius of 2,000 m around the injection point. CO₂ starts to dissolve in the brine, and the free gas is completely dissolved after 6,000 years. The brine with dissolved CO₂ tends to migrate downward as it has approximately 10 kg/m³ larger density than brine without CO₂. The brine containing dissolved CO₂ is carried downward and is replaced by brine with less CO₂. After 10,000

years, a large volume near the bottom of the formation contains brine with dissolved CO₂ out to a radius of 4,000 m.

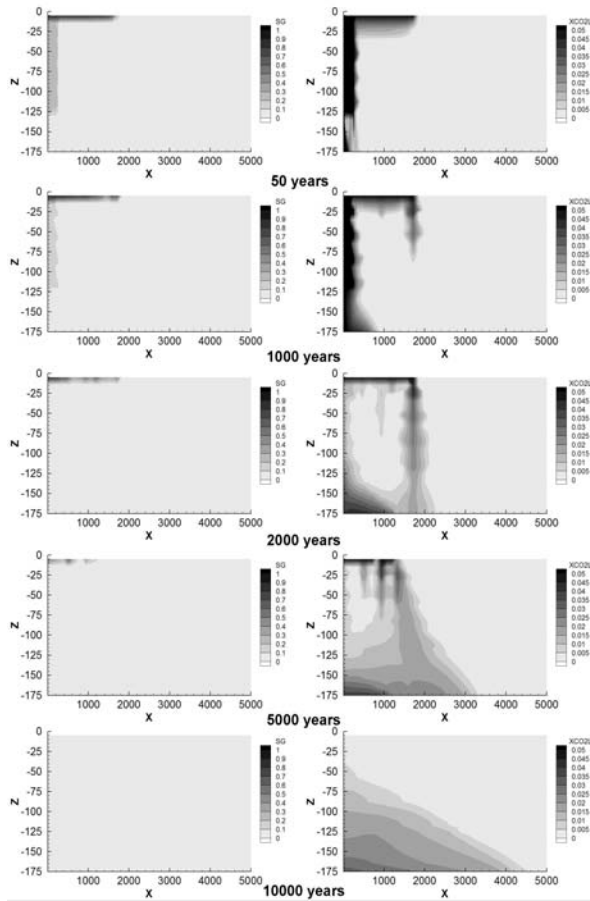


Figure 4. Supercritical CO₂ gas phase (SG) migration and mass fraction of the dissolved CO₂ in the brine (XCO₂L) simulated from 50 years after injection until 10,000 years.

Geochemical reactivity

Figure 5 shows that dissolution of CO₂ increases the acidity of the brine, which is buffered by carbonate dissolution so that the pH stabilizes at a value of 5.13. This pH value prevails in the region of ascending flow of supercritical CO₂ (500 years), is subsequently established in a region just below the cap rock (between 500 and 1,000 years), and subsequently extends downward (5,000 years). After 10,000 years low pH values are encountered mainly at the base of the reservoir close to the injection point. One can notice also that in the shale layers initial pH values are rising faster than in the sand layers, which is reinforced by the fact that the initial pH in the shales is higher than in the sands. Due to the fact that the porosity in the shales is much lower, the amount of dissolved CO₂ in the pores is also

lower, allowing it to be consumed much faster than in the sands, and causing pH to increase. This latter effect is crucial for interpreting the geochemical interactions, as will be seen below.

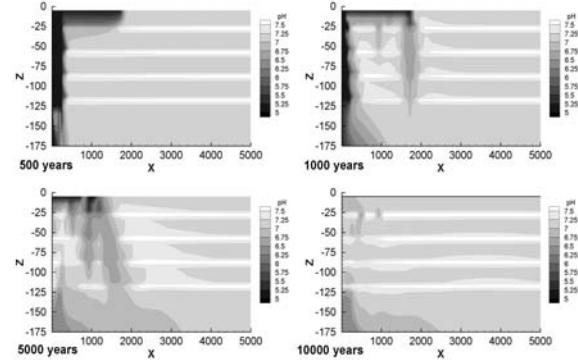


Figure 5. pH evolution after 500, 1000, 5000 and 10000 years, following 25 years of injection of supercritical CO₂.

Four main types of interactions can be identified.

Calcite dissolution and precipitation

Calcite dissolution occurs mainly in the region above the injection point and at the top of the reservoir just below the cap rock, that is where CO₂ rich brine is present that triggers acid attack on the carbonates. Calcite precipitation occurs also at low pH in all the shales cross-cut by the main up-flow zone above the injection point, as well as in the top shale layer where brine with low pH is convecting downward. The precipitation of calcite in the shales is a consequence of sand-shale cross-flow and a slight pH difference between the shales and the sands (as indicated in the batch results in Audigane et al., 2006). Downward flow of brine mobilizes Ca through calcite dissolution in the sands, which leads to super-saturation with respect to calcite when this brine subsequently passes through a shale layer with a slightly higher pH. As a consequence the Ca concentration in the brine declines, providing for additional calcite dissolution when the brine enters the next sand layer below. The effect is most pronounced in the top shale (Figure 6), because the acidity of the brine diminishes overall as it migrates downward, reducing its ability to dissolve calcite in the sands.

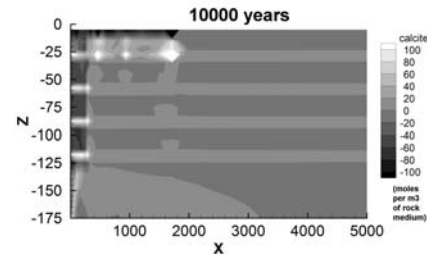
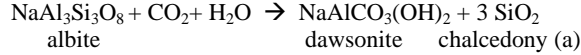


Figure 6. Calcite mineral evolution.

Additional calcite precipitation occurs at a later stage near the base of the reservoir where pH slowly increases due to CO₂ consumption in other reactions (see below), thereby increasing the saturation index of calcite.

Albite alteration

The second CO₂ trapping reaction is the alteration of albite, leading to the formation of dawsonite and chalcedony:



with some alteration in the sands (up to 10 moles per m³ of rock medium), and stronger alteration in the shales (up to 80 moles per m³ of rock medium, Figure 7).

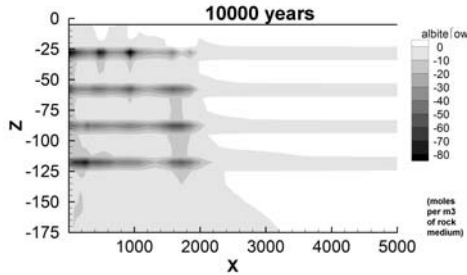


Figure 7. Albite mineral evolution.

Alteration is most intense in the downward limbs of brine convection and in the shale layers. However the formation of chalcedony (Figure 8) and dawsonite (Figure 9), which are the reaction products of albite alteration, occurs mainly in the sands (up to 35 and 80 moles per m³ of rock medium respectively).

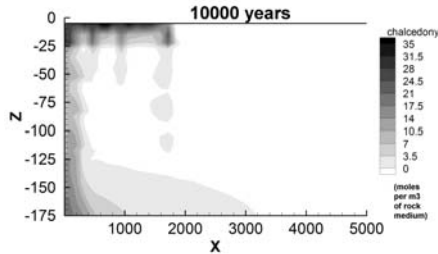


Figure 8. Chalcedony mineral evolution.

No dawsonite precipitation occurs in the shales, and the precipitation of chalcedony there is linked to other reactions (see below). Due to the convective flow regime, dissolution and precipitation processes are separated in space.

Both SiO₂ and Na are mobilized through albite dissolution in the shales and are re-precipitated as dawsonite and chalcedony in the sands in regions where pH is low.

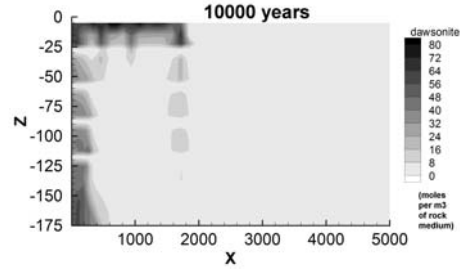
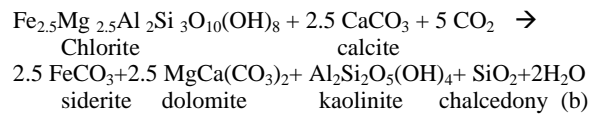


Figure 9. Dawsonite mineral evolution.

Chlorite alteration

The alteration of chlorite consumes calcite and results in the trapping of CO₂:



Both Fe and Mg act as donor cations for the trapping of CO₂ in the form of siderite and dolomite. Kaolinite is also formed but provides no trapping capacity for CO₂. Chlorite dissolution (Figure 10) occurs mainly in the shales in the low pH areas, where the main downward convection cross-cuts the shales.

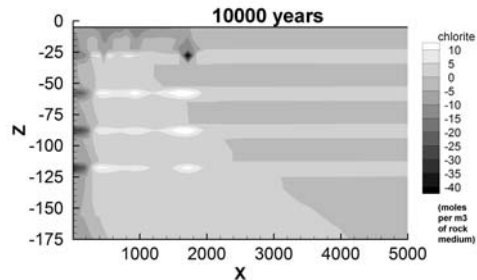


Figure 10. Chlorite mineral evolution.

Chlorite dissolution leads to the precipitation of kaolinite and siderite (reaction b), and a strong correlation exists with the precipitation patterns for these minerals (Figure 11 and Figure 12 respectively). In this case dissolution and precipitation are not spatially separated as had been the case for the albite alteration. However, the increased Mg from the dissolution of chlorite is mobilized away from the clay layers. As a consequence, no dolomite precipitation takes place, which is different from the batch model (Audigane et al., 2006). The chlorite dissolution pattern is strongly correlated with the calcite precipitation pattern. Indeed in shales where high Ca concentrations are present, chlorite dissolution is stimulated (reaction b). Also in the sands the saturation point for dolomite is not reached, and elevated Mg concentrations are maintained.

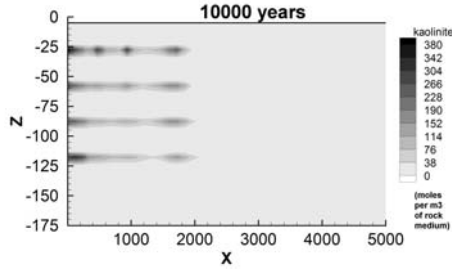


Figure 11. Kaolinite mineral evolution.

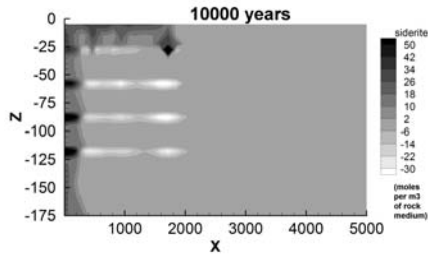
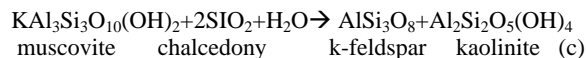


Figure 12. Siderite mineral evolution.

The dissolution of chlorite is strongly dependent on the pH. When pH rises, the reaction can proceed in the reverse direction, leading to the precipitation of chlorite and the dissolution of siderite and kaolinite. This can be observed in some regions of the descending brine, with more intense re-precipitation in the intercalating clay layers (up to 10 moles per m³ of rock medium). The re-precipitation is aided by elevated Mg concentration in the brine and does not occur in shales where high Ca concentrations are present due to calcite dissolution in the overlying sand layer.

Muscovite alteration

The alteration of muscovite described by the reaction:



is only indirectly linked to CO₂ interactions, in that it does not consume CO₂, but is favored by increased SiO₂ concentrations in the brine that arise from albite or chlorite alteration. Muscovite dissolution occurs mainly in the shale layers and is strongly correlated with the albite dissolution pattern (Figures 10 and 13). Muscovite alteration leads to the precipitation of kaolinite which is confirmed by a strong correlation with the precipitation pattern (Figure 11).

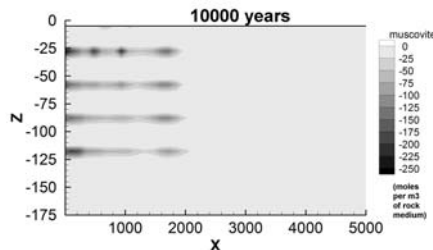


Figure 13. Muscovite mineral evolution.

Furthermore, muscovite alteration induces the precipitation of k-feldspar as was noted in the batch model for the shale (Audigane et al., 2006). Although k-feldspar precipitates in the shales (Figure 14), a large fraction of the K is mobilized and transported downward, leading to some k-feldspar precipitation in the adjacent sand layers.

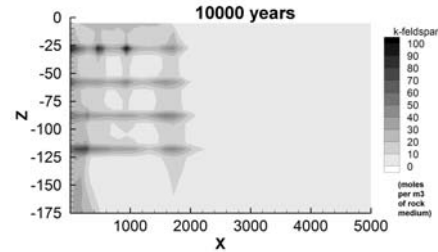


Figure 14. K-feldspar mineral evolution

Some background chemical reactivity is noticeable as well, due to the initial disequilibrium between the brine composition and the formation water. This activity includes minor calcite and chlorite precipitation, and albite dissolution in the shales.

Audigane et al. (2006) performed a mass balance of the amount of carbon dioxide present as supercritical phase, dissolved in the brine and transformed in minerals during the simulations showing that mineral trapping plays only a minor role, although it increases slowly with time and therefore contributes to long-term stability of the storage process. At the end of the simulation (10,000 years), no gaseous CO₂ remains in the aquifer. Approximately 5 % of the injected mass has been taken up by minerals, while the remaining 95 % has been dissolved in the brine.

CONCLUSIONS

A 2D radially symmetric reactive chemical transport model for the Sleipner CO₂ injection project has been developed. A 25 year injection period was simulated followed by a 10,000 year storage period that allowed to describe the evolution of the three main trapping processes of carbon dioxide: structural, dissolution and mineral trapping. The system was modeled as consisting of alternating highly permeable sands, separated by semi-permeable shales with different mineralogy.

Our simulations indicate that the geochemical reactivity of the Utsira formation is rather low, so that mineral trapping makes only minor contributions to CO₂ storage. Solubility trapping is shown to be the dominant long-term storage mechanism and is essentially complete after 5000 years. Physical and chemical heterogeneity play important roles in the geochemical evolution and associated changes in porosity. Our results suggest that the Utsira sand is

unlikely to undergo major chemical changes as a consequence of CO₂ injection.

REFERENCES

Arts, R., A. Chadwick, and O. Eiken, Recent time-lapse seismic data show no indication of leakage at the Sleipner CO₂ -injection site, Proceedings of the 7th International GHGT Conference, Cheltenham, UK, 2004.

Audigane, P., I. Gaus, I. Czernichowski-Lauriol, K. Pruess, and T. Xu, Two dimensionnal reactive transport modeling of CO₂ injection in a saline aquifer at the Sleipner site. Submitted to *American Journal of Sciences*, 2006.

Bjørlykke, K., T. Nedkvitne, R. Mogens, and C.S. Girish, 1992, Diagenetic processes in the Brent Group (Middle Jurassic) reservoir of the North Sea: an overview, in Morton, A.C., Haszeldine, R.S., Giles, M.R. and Brown, S., editors, *Geology of the Brent Group: Geological Society Special Publication*, v. 61, p. 263-287.

Bøe, R., and P. Zweigel, Characterization of the Nordland shale in the Sleipner area by XRD analysis, a contribution to the Saline Aquifer CO₂ Storage (SACS) project: Trondhiem, Norway, Confidential SINTEF Report 33.0764.00/01/01, 2001.

Czernichowski-Lauriol, I., B. Sanjuan, C. Rochelle, K. Bateman, J. Pearce, and P. Blackwell, Inorganic geochemistry, Chapter 7 in, *The underground disposal of carbon dioxide*, S. Holloway, editor: Final Report CT92-0031 of JOULE II Project, 1996.

Gaus, I., M. Azaroual, and I. Czernichowski-Lauriol, Reactive transport modeling of the impact of CO₂ injection on the clayey cap rock at Sleipner (North Sea): *Chemical Geology*, v. 217, p. 319-337, 2005.

Kemp, S.J., J.M. Pearce, and J. Steadman, Mineralogical, geochemical, and petrographical characterization of Nordland Shale cores from well 15/9-A-11, Sleipner field, northern North Sea: British Geological Survey Commissioned Report, CR/02/313., 40 p, 2002.

Lasaga, A.C., Chemical kinetics of water-rock interactions: *Journal of Geophysical Research*, v. 89, p. 4009-4025, 1984.

Narasimhan, T.N., and P.A. Witherspoon, An integrated finite difference method for analyzing fluid flow in porous media: *Water Resources Research*, v. 12, p. 57-64, 1976.

Pearce, J.M., S.J. Kemp, and P.D. Wetton, Mineralogical and petrographical characterization of 1m core from the Utsira formation, Central North Sea: British Geological Survey, Report WG/99/24C, 1999.

Pruess, K., TOUGH2 – a general-purpose numerical simulator for multiphase fluid and heat flow: Lawrence Berkeley Laboratory Report LBL-29400, Berkeley, California, 1991.

Pruess, K., and J. García, Multiphase flow dynamics during CO₂ disposal into saline aquifers: *Environmental Geology*, v. 42, p. 282-295, 2002.

Rochelle, C.A., and Y.A. Moore, The solubility of supercritical CO₂ into pure water and synthetic Utsira porewater: British Geological Survey Report CR/02/052, 2002.

SACS2, Final Technical Report: EU-contract ENK6-CT-1999-00014, 2002.

Sonnenthal, E.L., and N. Spycher, Drift-Scale coupled processes (DST and THC seep-age) models: AMR N0120/U0110 Rev.01, Yucca Mountain Project, Berkeley, California, Lawrence Berkeley National Laboratory Report, 2001.

Torp, T.A., and J. Gale, Demonstrating storage of CO₂ in geological reservoirs: the Sleipner and SACS projects: Proceedings of the GHGT 7 Conference: Kyoto, Japan, 1-4 October, 2002.

Xu, T., and K. Pruess, Modeling multiphase non-isothermal fluid flow and reactive geochemical transport in variably saturated fractured rocks: 1. Methodology: *American Journal of Science*, v. 301, p. 16-33, 2001.

Xu, T., J. Apps, and K. Pruess, Mineral sequestration of a sandstone-shale system: *Chemical geology*, v. 217, (3-4), p. 295-318, 2005.

Yeh, G.T., and V.S. Tripathi, A model for simulating transport of reactive multi-species components: Model development and demonstration: *Water Resource Research*, v. 27, p. 3075-3094, 1991.